Application of Cavity Maxwell Garnett Theory in SPR Based Fiber Optic Sensor with Porous Alumina Structure

Jyoti -
Central University of Rajasthan
R. K. Verma (rkverma@curaj.ac.in)
Central University of Rajasthan

Research Article

Keywords: anoporous alumina, Cavity Maxwell Garnett theory, nanolayer.

Posted Date: September 15th, 2021

DOI: https://doi.org/10.21203/rs.3.rs-796961/v1

Application of Cavity Maxwell Garnett theory in SPR based fiber optic sensor with porous alumina structure

Jyoti and R. K. Verma*

Department of Physics, Central University of Rajasthan

NH-8 Bandarsindri, Ajmer-305817 (India)

Abstract

The present manuscript describes the theoretical understanding of nanoporous alumina based fiber optic sensing structures. The Cavity Maxwell Garnett theory is used to calculate the dielectric functions of the proposed layer. The performance of the proposed sensing structure is evaluated in terms of its sensitivity towards change in the refractive index of the nearby medium. The sharpness of the resonance has also been calculated as an estimation of the performance parameters. It has been observed that the proposed structure is approximately thirteen times more sensitive than the conventional fiber optic sensors. The study has further been extended by replacing the nanolayer of Alumium with the nanolayer of the gold. A comparative study has been provided in terms of the efficiency of the fiber optic probe. The effects of change in pore radius, thickness of the adsorbed medium and shell radius have also been studied.

***Corresponding Author Email:** rkverma@curaj.ac.in

1. Introduction

The application of surface plasmons (SPs) in sensing is a rapidly growing field and is upgrading its performance in chemical sensing, environmental monitoring, foodborne screening, medical diagnostics and gas sensing continuously [1-5]. Surface plasmons are visualized as the coherent oscillations of free electrons on the metal dielectric interface [6]. For the occurrence of resonance between surface plasmon waves and evanescent waves a specific configuration is required. This configuration was firstly introduced by Kretschmann, in which a very high refractive index prism is coated by a thin layer of metal film on its base. In such configuration the wave vector of evanescent wave become equal to the wave vector of surface plasmon wave at a particular angle of incident light so that resonance condition is satisfied. A sharp fall is observed in the reflected power spectrum owing to this resonance effect. The shift in dip position with the change of refractive index of local dielectric medium is a crucial key for sensing applications [7-9]. Yee and Jorgenson replaced the basic Kretschmann configuration of prism with an optical fiber [10]. Fiber based optical sensors have several advantages over prism-based sensors. This makes sensors miniaturized, shock free, mobile and have low cost. In fiber optic based SPR sensors small portion of cladding is removed from the middle portion of fiber and then is coated with a thin layer of plasmonic material Ag or Au in general. Subsequently a polychromatic light is launched from one end of the fiber such that the light gets guided using TIR phenomenon on the interface of its core and cladding [11]. This has some additional advantages in remote sensing and online monitoring [12]. Fiber optic with Bragg grating and long period grating written on its core are also being used for the enhancement of its performance parameters [13-14].

To foster the performance of fiber optic based SPR sensors, numerous studies have been carried out by using different metals for thin film deposition, nanostructures like nanorods, nanospheres, nanoporous structure and many others. An overlayer of an additional

nanostructure ameliorates the performance of the conventional fiber optic based SPR sensors. The material for the selection of nanostructure should be chemically inert, non-degradable and thermally stable [15-16]. Alumina fulfils all these conditions and formation of nanoporous alumina structure is less expensive and quite easy. Synthesis of nanoporous material by using electro-chemical techniques have various optical applications in SPR, Raman spectroscopy, reflective interference and in waveguides [17]. This technique has several advantages like highly ordered nanochannel array and have vertical alignment of cylindrical pores. Nanoporous anodic alumina (NAA) is an optimum example of this technique which has distinct chemical, optical and mechanical properties as well as good thermal stability and high surface to volume ratio [18]. NAA has self-ordered, homogeneous and honeycomb like structure. Its geometrical parameters like pore diameter, interpore distance and length of pore can be tuned by changing anodization condition like temperature, current, anodization voltage, electrolyte, composition of electrolyte and time. It has chemical inertness and ability to protect itself from self-degradation [19-21]. Porous structure of NAA has high surface to volume ratio which helps in adsorption of more sensing medium. It has multiple applications in bio-sensing, filtration, soler cells, data storage, drug delivery, template synthesis, humidity and gas sensing [22-26]. Further, to evaluate the optical properties of nanostructures the calculation of dielectric function is a major parameter for inhomogeneous mixture of dielectric materials. Several effective medium theories like Bruggeman, Monache, Landau- Lifshitz/Looyenga, Bergman representation and Cavity Maxwell Garnett effective medium theory can be used to calculate effective dielectric function [27-32]. For nanoporous structure Cavity Maxwell Garnett theory is most suitable which considers the effect of three inhomogeneous materials. In our case we will consider the effect of three layers viz. metal layer, nanoporous alumina and air [33].

In the present study, we proposed SPR based fiber optic sensor in which fiber core is coated with a nanolayer of aluminium metal with an additional nanoporous alumina layer coated on it. Additionally, since gold is also compatible to couple with nanoporous alumina layer [34], therefore the study has been extended to see the effect of replacing aluminium nanolayer with gold nanolayer. A comparison between the performance parameters of sensor is analysed for both aluminium and gold with porous alumina on to the top of it. The proposed structure with nanoporous alumina film enhances the sensitivity to approximately 13 times to their conventional aluminium and gold configuration. It is also observed that the gold based configuration has better sensitivity than aluminium based configuration though the sharpness of resonance is better in case of aluminium.

2. Structure Details

In SPR based fiber optic sensor, a small portion of cladding is removed from the central region of the fiber core. For the excitation of surface plasmon wave using Kretschmann configuration a thin metal layer is deposited over this uncladded portion of the core (Conventional structure). An aqueous based sensing medium is place over this metal layer. However in the proposed structure we further coat this metal layer with porous alumina structure that will be surrounded by the medium to be sensed (Proposed structure) as shown in fig.(1). A polychromatic light is introduced from one end of the fiber and a transmitted spectrum is recorded from the other end. A sharp dip in the transmitted spectra corresponding to the refractive index of the sensing medium is observed. The shift in dip position corresponding to the change in the sensing medium makes this configuration useful for sensing applications. In fiber based configuration, wavelength interrogation method is used in general [35].

2.1 Dispersion Relations

In our simulations fused silica fiber is considered for which Sellemeir dispersion relation is [36]:

$$n_1(\lambda) = \sqrt{1 + \frac{a_1 \lambda^2}{\lambda^2 - b_1^2} + \frac{a_2 \lambda^2}{\lambda^2 - b_2^2} + \frac{a_3 \lambda^2}{\lambda^2 - b_3^2}} \quad (1)$$

here, Sellemeir coefficients are $a_1 = 0.6961663,\ a_2 = 0.4079426,\ a_3 = 0.8974794,\ b_1 = 0.0684043,\ b_2 = 0.1162414$ and $b_3 = 9.896161$ and the wavelength values are in micrometres and n_1 is the refractive index of fiber core.

For metal layer we are choosing aluminium and gold taking care of performance parameters since gold has better sensitivity and aluminium has better sharpness of the resonance in conventional case. The Drude dispersion relation for metal dielectric function is expressed as [37]:

$$\varepsilon_2(\lambda) = 1 - \frac{\lambda^2}{\lambda_p^2(\lambda_c + i\lambda)} \quad (2)$$

here λ_p is the plasma wavelength and λ_c is collision wavelength in metals and λ is the wavelength that lies in the range of visible and IR spectra. Plasma and collision wavelength constants for aluminium and gold are taken from the reference [37].

Further, in our proposed configuration we are using nanoporous aluminium oxide because of its various applications in molecular separation, energy generation, catalysis, electronics, photonics, sensors, storage and biosensors also [38]. Nanoporous anodic alumina (NAA) fabrication is simple and economical with the process of self-ordering of nano-pores which do not even call for lithography and the end result are highly ordered [39-41]. NAA has close packed structure of hexagonal arrays having nanopores aligned perpendicular to the surface

of substrate material. The pore geometry can be controlled by applied potential [42-44], type of electrolyte [45-47], composition of electrolyte [47], PH [47], current [48-49] and temperature [50] to achieve the desired pore size and interpore distance. NAA has incredible properties like chemical and thermal stability, more surface area and hardness.

2.2 Cavity Maxwell Garnet Theory

Dielectric function is one of the major parameter to calculate optical properties like reflectance and transmittance [51]. In the study of inhomogeneous mixture of dielectric materials which have dimensions small in comparison of wavelength the dielectric function has a notion of nanostructure of the dielectric material. The two effective models which are most used are Bruggeman [52] and Maxwell Garnett theories [53]. Maxwell Garnett model is further having two types one is Spherical Maxwell Garnett (SMG) and another is Cavity Maxwell Garnett (CMG). In SMG, spherical inclusion is filled with material like metal oxides and air must be filled outside. In CMG, air inclusions are spherical and material is coated outside of it as depicted in fig.(2). Afterward, various modification is done to these effective medium theories, because the voids are not always spherical sometimes these may be elongated and cylindrical. SMG model is less explored than CMG because of its undesired result of spectra [51]. So further study was done on CMG in which the characteristics of damping of phonons on bulk surface are different from phonon characteristics into the bulk material. Weaver et. al. [54] and others [55] remodel the CMG model which consists of three dielectric materials in which two of them are related (like metal and metal oxide) and one is air. For different topology/geometry damping characteristics of phonon is different. Shell layer represents the sensing medium layer and its thickness, plasma frequency, rate of phonon damping affects the reflectance and transmittance of spectra. NAA consists three constituent materials in which alumina is considered as surrounding medium, sensing medium present on

the walls of pore and air is filled in open space of pore [56]. The effective contribution of these is given by following formula [57]:

$$\varepsilon_{eff} = \frac{fA_c\rho^3 + f\varepsilon_s A_s(1-\rho^3) + \varepsilon_{Al_2O_3}(1-f)}{fA_c\rho^3 + fA_s(1-\rho^3) + 1 - f} \quad (3)$$

where,

$A_c = 3\varepsilon_s B,\ A_s = (3 + 2\varepsilon_s)B,\quad \rho = \frac{r_p}{r_s}$ and

$$B = \frac{3\,\varepsilon_{Al_2O_3}}{(\varepsilon_s + 2\,\varepsilon_{Al_2O_3})(2\varepsilon_s + 1) - 2(\varepsilon_s - \varepsilon_{Al_2O_3})(\varepsilon_s - 1)\rho^3} \quad (4)$$

where, ε_s = dielectric constant of shell (adsorbed molecules on the walls of the pore).

r_p = pore radius, r_s = shell radius and f is the pore volume fraction, which is given for cylindrical pore and shell,

$$f = \frac{\text{volume of pore}}{\text{volume of shell}}; \quad (5)$$

and, $\varepsilon_{Al_2O_3}$ is the dielectric constant of the aluminium oxide which is given as [58]:

$$\varepsilon_{Al_2O_3}(\lambda) = 1 + \frac{s_1\lambda^2}{\lambda^2 - t_1^2} + \frac{s_2\lambda^2}{\lambda^2 - t_2^2} + \frac{s_3\lambda^2}{\lambda^2 - t_3^2} \quad (6)$$

and $s_1 = 1.4313493,\ s_2 = 0.65054713, s_3 = 5.3414021, t_1 = 0.0726631, t_2 = 0.1193242, t_3 = 18.028251.$

Further, for the calculation of transmitted power we have used N-layer matrix method for stratified media has been used [59].

3. Performance Parameters

The performance of the fiber optic SPR sensor is analyzed in terms of sensitivity, full width half maximum (FWHM) and the sharpness of resonance. In the wavelength interrogation mode, the resonance wavelength λ_{res} corresponds with refractive index n_s of sensing

medium. Variation in the refractive index of sensing medium leads to the change in its resonance wavelength. Therefore, the sensitivity can be calculated as the ratio of change of resonance wavelength $\Delta\lambda_{res}$, with the variation of refractive index of the sensing medium Δn_s [59]

$$\text{Sensitivity} = \frac{\Delta\lambda_{\text{res}}}{\Delta n_s} \tag{7}$$

The FWHM can be determined by calculating the full width at half maximum of the resonance curve ($\Delta\lambda_{0.5}$), expressed as:

$$FWHM = \Delta\lambda_{0.5}, \tag{8}$$

Sharpness of the resonance is defined as the reciprocal of FWHM.

$$\text{Sharpness of resonance} = \frac{1}{\text{FWHM}} \tag{9}$$

4. Result and Discussion

In the present simulation, we have considered silica-based fiber core of diameter 600 μm and 0.5 cm of uncladded portion as a sensing region which is preferably placed in the middle of the fiber. To enhance the performance parameters of the sensor we put an overlayer of porous alumina on the nanofilm of metal layer. We present a comparison of performance parameters of conventional aluminium based configuration (fiber + aluminium film + sensing medium) with the proposed version with an additional nanoporous alumina layer (fiber + aluminium film + nanoporous alumina + sensing medium). In another case, we consider conventional gold-based configuration (fiber + gold film + sensing medium) and compared with the proposed version (fiber + gold film + porous alumina+ sensing medium) (Figure 3 and 4). The holes in the nanoporous alumina are termed as shells of definite radius. After the adsorption of the sensing medium on to the inner walls of the shell the empty space is called

as the pore. The difference between the shell radius and the pore radius is the thickness of the medium that has been adsorbed on to the walls of the shell. We have considered Aluminum film thickness of 45 nm and gold film thickness as 50 nm. For both the cases we have examined the refractive indices of aqueous based sensing medium in the range of 1.333 to 1.337 with a difference of 0.001 (five samples), since most of the bio-analytes are aqueous based and have similar refractive indices.

4.1 Conventional Structure: In figure 5 and 6, we observed two resonance dips corresponding to the refractive indices 1.333 and 1.337 in transmitted power for conventional Aluminum and Gold structures and the shift in resonance dip is quite small that leads to smaller sensitivity.We have calculated sensitivity for this configuration which is 2 μm/RIU and for conventional gold structure it is 3.5 μm/RIU. Sharpness of the resonance was also calculated for the conventional aluminium and gold configuration and is 0.4 μm^{-1} and 0.0769 μm^{-1}. Aluminium and gold are considered because aluminium have large sharpness of resonance and gold leads to higher sensitivity as reported in many research articles.

4.2 Proposed Structure Analysis: To realize the proposed structure the basic conventional structure is coated with an overlayer of porous alumina because its porous structure increases surface to volume ratio which may boost up the adsorption of sensing medium. From figure 3 and figure 4 (enlarge view) it can be seen that we are dealing with small feasible size of shells on porous alumina so that we can get large number of shells in a fix area and more sensing medium can get adsorbed on the walls of shell. To plot the SPR curves for the proposed structure we have considered a fixed value of the shell radius as 0.0075 μm with the changing values of the pore radius (figure 7 and 8). Adsorbed layer thickness is the difference of shell radius and the pore radius. Further, in figure 9, the red shift in the resonance wavelength of the proposed configuration with Aluminum layer can be seen corresponding to the change in refractive index of sensing medium from 1.333 to 1.337. In this configuration the resonance

condition gets satisfied at higher value of wavelength than the conventional structure. The conventional structure works with wavelength of visible region only whereas in the proposed configuration resonance wavelength extends in IR range also. This change in resonance dip with the variation of refractive index represents sensitivity of the proposed sensor. Similarly, when we place gold nanofilm at the place of aluminium we observe that resonance condition gets satisfied at even higher wavelength for the same refractive indices than in case of Aluminum (figure 10). It is observed that red shift in transmitted spectra is more in case of gold than Aluminum. The maximum sensitivity is observed for the pore radius 0.00573 μm with adsorbed layer thickness of 0.00177 μm and the sensitivity value in this case for aluminum and gold nanofilm is 26 μm/RIU and 46.25 μm/RIU respectively which is approximately 13 times to their conventional structure (2 μm/RIU and 3.5 μm/RIU). This huge boost in the sensitivity is due to their larger shift in the resonance dip and creates a significant impact on the performance of the sensor. It is to be noted that the ssensitivity is more in case of Gold nanofilm than the Aluminium nanofilm as in conventional case. The physical reason behind this enhanced value of sensitivity could be the large adsorption of the sensing medium owing to the large surface area of the nanostructure.

In figure 11, the SPR curves observed for shell radius 0.0075 μm, pore radius 0.00573 μm and absorbed layer thickness 0.00177 μm which is also the case of maximum sensitivity for both Aluminium and gold are shown. Careful observation of these SPR curves reveal that the Aluminium nanofilm have sharp resonance dip than gold however the dip shift in gold is more than Aluminium and is also at higher wavelength.

4.3 Effect of Pore Radius

4.3.1 Sensitivity

Figure 12 shows the structural change with increase in pore radius for a fix value of shell radius and the corresponding decrease in the thickness of adsorbed layer of sensing medium. In figure 13, we have shown a comparison between the proposed configurations of Aluminum and gold with variation of pore size in the nanoporous structure of alumina. The fix value of shell radius is 0.0075 μm and the pore radius varies from 0.00573 μm to 0.0061 μm with decreasing thickness of the adsorbing layer. In proposed configuration, gold base structure has maximum sensitivity of 46.25 μm for pore radius 0.00573 μm and minimum sensitivity 4.5 μm/RIU, corresponding to the pore radius 0.0061 μm. In the case of Aluminium based proposed configuration, maximum sensitivity is 26 μm/RIU for pore radius 0.00573 μm and minimum sensitivity is 2.75 μm/RIU corresponding to pore radius 0.0061 μm. It has been observed that for the further increase in the radius of pore, sensitivity becomes nearly equal to their conventional structure. It can be concluded that the more is the thickness of adsorbed layer better is the sensitivity. If we further increase the adsorbed layer thickness beyond 0.00177 μm the resonance dip falls in mid infrared region where the dispersion relation for metals given by Drude model is not valid and if thickness of adsorbed layer is less than 0.00153 μm then sensitivity becomes approximately equal to their conventional configuration. Therefore, if the adsorption of the sensing layer on to the walls of the shell is very weak the sensitivity value will be poor as can been seen from Table 1.

4.3.2 Sharpness of Resonance

The sharpness of resonance is dependent on full width at half maximum (FWHM) of the SPR curve. In section 4.2 we have discussed that the gold configuration have broader resonance dip than Aluminum configuration and hence it is expected from equation 13 that

the sharpness of resonance for gold-based configuration is more than aluminium. From figure 14, it can be seen that for proposed aluminium configuration slope for the sharpness of resonance of aluminium is much higher than that of the gold based structure. In the proposed aluminium configuration, the highest sharpness of resonance is 250 μm^{-1} for pore radius 0.00593 μm and lowest sharpness of resonance is 30.3030 μm^{-1} for pore radius 0.00573 μm corresponding to the fix shell radius 0.0075 μm. For proposed gold configuration, highest sharpness of resonance is 55.55 μm^{-1} for the pore radius 0.00593 μm, and lowest sharpness of resonance is 3.4364 μm^{-1} for pore radius 0.00573 μm, for the same value of shell radius 0.0075 μm. Hence it can be concluded that the better is the adsorption of the sensing layer on to the walls of the shell poor will be the sharpness of the resonance. The numerical values of the sharpness of the resonance can be seen from Table 2.

4.4 Effect of Shell Radius

4.4.1 Sensitivity

So far we took the fixed radius of shell and changed the radius of pore due to which adsorbed layer thickness was changing. Further we have considered the fixed value of the adsorbed sensing layer thickness equal to 0.0018 μm and both shell and pore radius were varied (figure 15). We found that the highest sensitivity of the proposed aluminium configuration was 23.25 μm/RIU and for gold configuration it was 41.5 μm/RIU, corresponding to pore radius 0.00585 μm and shell radius 0.00765 μm. Least sensitivity of proposed aluminium and gold configurations were 2.5 μm/RIU and 4.25 μm/RIU corresponding to pore radius of 0.00705 μm and shell radius of 0.00885 μm as shown in figure 16 (Table 3). Further increase of pore and shell radius gave approximately similar sensitivity to their conventional structure and the nanoporous alumina layer is no longer useful. It is to be noted that in porous alumina structure, with the increase of shell radius for a

fix area and interpore distance the number of pores will be less and in the case of small pore sizes the number of pores will be large. Larger the number of pores means more material get adsorbed on the walls of pore leading to higher value of the sensitivity.

4.4.2 Sharpness of Resonance

The sharpness of resonance of proposed configurations has also been evaluated for fix thickness of adsorbed layer of sensing medium corresponding to increasing pore and shell radius. It can be seen from figure 17, the slope of the proposed aluminium configuration is much higher than that of the gold configuration because aluminium has sharper SPR dip than gold. The maximum sharpness of resonance was found to be 222.22 μm^{-1} and 74.07 μm^{-1} for proposed aluminium and gold configuration corresponding to pore and shell radius of 0.00705 μm and 0.00885 μm respectively. The numerical values can be read from Table 4.

4.5 Trade-off between sensitivity and sharpness of resonance

It can be noticed from the above discussion that there is a tradeoff relationship between performance parameters i.e. between sensitivity and the sharpness of the resonance. For the same value of pore radius we did not to get both high sensitivity and sharpness of resonance. To locate an optimum value of the pore radius for a reasonably good value of both the parameters we have plotted in figure 18, both the performance parameters with pore radius. From the intersection point of both the curves we got an optimum value of pore radius where both sensitivity and sharpness have moderately high value. The pore radius value of 0.00623 μm gave the optimum point where we got the sensitivity and sharpness of the resonance as 7.9 μm/RIU and 81.2865 μm^{-1} respectively for Aluminium based configuration. Similar to the case of aluminium, we located the optimum pore radius for the proposed gold configuration where both the sensitivity and sharpness of resonance can provide a moderately high value. From the figure 19, it can be seen that the pore radius 0.006434 μm the

moderately high values of sensitivity are 9 μm/RIU and sharpness of resonance 16.608 μm^{-1} respectively.

5. Conclusions

A rigorous analysis of the porous alumina based fiber optic sensor has been deliberated. A comparative analysis between the aluminum and gold based structures revealed that the sensitivity is better in case of gold based configuration as compared to aluminium based configuration. However in both the configurations, the sensitivity values are approximately thirteen times higher than their conventional counterparts. Further, the sharpness of the resonance has also been studied in detail and a trade-off relationship between the sensitivity and sharpness of the resonance has been observed. The optimum value of the pore radius has been located for both the configurations.

Acknowledgement: Ms. Jyoti would like to acknowledge Central University of Rajasthan for providing university fellowship. Also, this work is partially supported by DST SERB CRG/2020/005593, India.

REFERENCES:

[1] A. K. Sharma, R. Jha, B. D. Gupta, Fiber-optic sensors based on surface plasmon resonance: a comprehensive review, *Sens. J. IEEE* **7**, 1118 (2007).

[2] M. Piliarik, L. Parova, J. Homola, High-throughput SPR sensor for food safety, *Biosens. Bioelectron* **24**, 1399 (2009).

[3] H. Sipova, J. Homola, Surface plasmon resonance sensing of nucleic acids: A review, *Anal. Chim. Acta.* **773**, 9 (2013).

[4] J. Homola, Surface plasmon resonance sensors for detection of chemical and biological species, *Chem. Rev.* **108**, 462 (2008).

[5] A. K. Sharma, G.J. Mohr, Theoretical understanding of an alternating dielectric multilayer-based fiber optic SPR sensor and its application to gas sensing, *New J. Phys*. **10**, 023039 (2008).

[6] R. K. Verma, B. D. Gupta, Surface plasmon resonance-based fiber optic sensor for the IR region using a conducting metal oxide film, *Journal of the Optical Society of America A.* **27**, 846 (2010).

[7] Y. Chen, Y. Yu, X. Li, Z. Tan, Y. Geng, Experimental comparison of fiber optic surface plasmon resonance sensors with multi metal and single silver or gold layer, *Plasmonics* **10**, 1801 (2015).

[8] E. Fontana, Thickness optimization of metal films for the development of surface-plasmon-based sensors for nonabsorbing media, *Appl. Opt*. **45**, 7632 (2006).

[9] E. Kretschmann, Determination of the Optical Constants of Metals by Excitation of Surface Plasmons, *Z. Physik* **241**, 313 (1971).

[10] R. C. Jorgenson, S.S. Yee, A fiber-optic chemical sensor based on surface plasmon resonance, *Sens Act B* **12**, 213, (1993).

[11] S. K. Srivastava, B. D. Gupta, Fiber Optic Plasmonic Sensors: Past, Present and Future, *The Open Optics Journal* **7**, 58 (2013).

[12] R. Jha, R. K. Verma, B. D. Gupta, Surface plasmon resonance-based tapered fiber optic sensor: Sensitivity enhancement by introducing a teflon layer between core and metal layer, *Plasmonics* **3**, 151 (2008).

[13] Y. Ma, G. Farrell, Y. Semenova, H.P. Chan, H. Zhang, Q. Wu, Sensitivity enhancement for a multimode fiber sensor with an axisymmetric metal grating layer, *Photon. Nanostruct. Fundam. Appl.* **12**, 69 (2014).

[14] S. M. Tripathi, A. Kumar, E. Marin, J.P. Meunier, Side-polished optical fiber grating-based refractive index sensors utilizing the pure surface plasmon polariton, *Lightwave Technol* **26**, 1980 (2008).

[15] L. Vojkuvka, A. Santos, J. Pallarès, J. Ferré-Borrull, L. F. Marsal, J.-P. Celis, On the mechanical properties of nanoporous anodized alumina by nanoindentation and sliding tests, *Surf. Coat. Technol.* **206**, 2115 (2012).

[16] L. F. Marsal, L. Vojkuvka, P. Formentin, J. Pallarés, J. Ferre-Borrull, Fabrication and optical characterization of nanoporous alumina films annealed at different temperatures, *Opt. Mater.* **31**, 860 (2009).

[17] A. Santos,T. Kumeria,D. Losic, Nanoporous anodic aluminum oxide for chemical sensing and biosensors, *Trends Anal. Chem.* **44**, 25 (2013).

[18] R. E. Gyurcsanyi, Chemically-modified nanopores for sensing, *Trends Anal. Chem.* **27**, 627, (2008).

[19] A. Ghicov, P. Schmuki, Self-ordering electrochemistry: A review on growth and functionality of TiO_2 nanotubes and other self-aligned MO_x structures. *Chem. Commun.*, 2009, 2791-2802 (2009).

[20] W. Lee, R. Ji, U. Gösele, K. Nielsch, Fast fabrication of long-range ordered porous alumina membranes by hard anodization. *Nat. Mater.* **5**, 741 (2006).

[21] A. Santos, P. Formentín, J. Pallarès, J. Ferré-Borrull, L.F. Marsal, Structural engineering of nanoporous anodic alumina funnels with high aspect ratio. *J. Electroanal. Chem.* **655**, 73 (2011).

[22] T. Kumeria, A. Santos, D. Losic, Nanoporous Anodic Alumina Platforms: Engineered Surface Chemistry and Structure for Optical Sensing Applications, *Sensors* **14**, 11878 (2014).

[23] D. Losic, M. Lillo, Porous alumina with shaped pore geometries and complex pore architectures fabricated by cyclic anodization, *Small* **5**, 1392 (2009).

[24] W. Lee, K. Schwirn, M. Steinhart, E. Pippel, R. Scholz, U. Gösele, Structural engineering of nanoporous anodic aluminium oxide by pulse anodization of aluminium. *Nat. Nanotechnol.* **3**, 234 (2008).

[25] G. Meng, Y.J. Jung, A. Cao, R. Vajtai, P.M. Ajayan, Controlled fabrication of hierarchically branched nanopores, nanotubes, and nanowires, *Proc. Natl. Acad. Sci. USA* **102**, 7074 (2005).

[26] D. Losic, D. Preparation of porous anodic alumina with periodically perforated pores, *Langmuir* **25**, 5426 (2009).

[27] D. A. G. Bruggeman, Calculation of various physical constants of heterogeneous substances. III. The elastic constants of quasiisotropic mixtures of isotropic substances, *Ann. Phys. (Leipzig)* **24**, 636 (1935).

[28] L. D. Landau and E. M. Lifshitz, Electrodynamcis of Continuous Media, *Journal of Physical Society of Japan* **16**, 359 (1961).

[29] H. Looyenga, Dielectric constants of heterogeneous mixtures, *Physica (Amsterdam)* **31**, 401 (1965).

[30] J. C. Maxwell Garnett, Colours in metal glasses and in metallic films, *Philos. Trans. R. Soc. London, Ser. A* **203**, 385, (1904).

[31] J. Monecke, Bergman spectral representation of a simple expression for the dielectric response of a symmetric two-component composite, *J. Phys.: Condens. Matter* **6**, 907 (1994).

[32] D. J. Bergman, Exactly Solvable Microscopic Geometries and Rigorous Bounds for the Complex Dielectric Constant of a Two-Component Composite Material, *Phys. Rev. Lett.* **45**, 148, (1980).

[33] J. E. Spanier and I. P. Herman, Use of hybrid phenomenological and statistical effective-medium theories of dielectric functions to model the infrared reflectance of porous SiC films, *Phys. Rev. B* **61**, 10437 (2000).

[34] P. Evans, W. R. Hendren, R. Atkinson, G. A. Wurtz, W. Dickson, A. V. Zayats, and R. J. Pollard, Growth and properties of gold and nickel nanorods in thin film alumina, Nanotechnology **17**, 5746 (2006).

[35] J. Homola, On the sensitivity of surface plasmon resonance sensors with spectral interrogation, *Sens. Actuators B* **41**, 207 (1997).

[36] A. K. Ghatak, K. Thyagarajan, Introduction to fiber optics (Cambridge: Cambridge University Press) 1998.

[37] A.K. Mishra, S.K. Mishra, R.K. Verma, Graphene and Beyond Graphene MoS_2: A New Window in Surface-Plasmon-Resonance-Based Fiber Optic Sensing, *The Journal of Physical Chemistry C* **120**, 2893 (2016).

[38] A. M. M. Jani, D. Losic, N. H. Voelcker, Nanoporous anodic aluminium oxide: Advances in surface engineering and emerging applications, *Progress in Material Science* **58**, 636 (2013).

[39] A. Ghicov, P. Schmuki, Self-ordering electrochemistry: A review on growth and functionality of TiO2 nanotubes and other self-aligned MO_x structures. *Chem. Commun*., 2791 (2009). No volume number

[40] R. B. Wehrspohn, Ordered porous nanostructures and applications, *Nanostructure science and technology, Springer* **1**, 207 (2005).

[41] Y. Ren, Z. Ma, P.G. Bruce, Ordered mesoporous metal oxides: synthesis and applications, *Chem Soc. Rev*. **41**, 4909 (2012).

[42] L. Woo, K. Jae-Cheon, Highly ordered porous alumina with tailor-made pore structures fabricated by pulse anodization, *Nanotechnology* **21**, 485304 (2010).

[43] L. Yi, L. Zhiyuan, C. Shuoshuo, H. Xing and H. Xinhua, Novel AAO films and hollow nanostructures fabricated by ultra-high voltage hard anodization, *Chem. Commun.* **46**, 309 (2009).

[44] F. Zhang, X. Liu, C. Pan and J. Zhu, Nano-porous anodic aluminium oxide membranes with 6–19 nm pore diameters formed by a low-potential anodizing process, *Nanotechnology* **18**, 345302 (2007).

[45] A.L. Friedman, D. Brittain, L. Menon, Roles of pH and acid type in the anodic growth of porous alumina, *J. Chem. Phys.* **127**, 154717 (2007).

[46] S. Z. Chu, K. Wada, S. Inoue, M. Isogai, Y. Katsuta, A. Yasumori, Large-scale fabrication of ordered nanoporous alumina films with arbitrary pore intervals by critical-potential anodization, *J Electrochem. Soc.* **153,** 384 (2006).

[47] S. Ono, M. Saito, H. Asoh, Self-ordering of anodic porous alumina formed in organic acid electrolytes, *Electrochimica. Acta*. **51**, 827 (2005).

[48] K. Lee, Y. Tang, M. Ouyang, Self-ordered controlled structure nanoporous membranes using constant current anodization, *Nano. Lett*. **8**, 4624 (2008).

[49] W. Lee, J. C. Kim, U. Gösele, Spontaneous current oscillations during hard anodization of aluminum under potentiostatic conditions, *Adv. Funct. Mater* **20**, 21 (2010).

[50] G.D. Sulka, W. J. Stepniowski, Structural features of self-organized nanopore arrays formed by anodization of aluminum in oxalic acid at relatively high temperatures. *Electrochimica. Acta.* **54**, 3683 (2009).

[51] J. E. Spanier, I. P. Herman, Use of hybrid phenomenological and statistical effective-medium theories of dielectric functions to model the infrared reflectance of porous SiC films, *Phys. Rev. B* **61**, 10437 (2000).

[52] D. A. G. Bruggeman, Calculation of various physical constants of heterogeneous substances. I. Dielectric constants and conductive capabilities of the mixing bodies of isotropic substances, *Ann. Phys. (Leipzig)* **24**, 636 (1935).

[53] J. C. Maxwell Garnett, Colours in metal glasses and in metallic films, *Philos. Trans. R. Soc. London Ser. A* **203**, 385 (1904).

[54] J. H. Weaver, R. W. Alexander, L. Teng, R. A. Mann, and R. J. Bell, Infrared absorption of small silicon particles with oxide overlayers, *Phys. Status Solidi A* **20**, 321 (1973).

[55] Y. Sasaki, Y. Nishina, M. Sato, and K. Okamura, Optical-phonon states of SiC small particles studied by Raman scattering and infrared absorption, *Phys. Rev. B* **40**, 1762 (1989).

[56] A. G. Koutsioubas, N. Spiliopoulos, D. Anastassopoulos, A. A. Vradis, G. D. Priftis, Nanoporous alumina enhanced surface plasmon resonance sensors, *Journal of Applied Physics* **103**, 094521 (2008).

[57] J. E. Spanier, I. P. Herman, Use of hybrid phenomenological and statistical effective-medium theories of dielectric functions to model the infrared reflectance of porous SiC films, *Phys. Rev. B* **61**, 10437 (2000).

[58] R. Tabassum and B. D. Gupta, Influence of Oxide Overlayer on the Performance of a Fiber Optic SPR Sensor with Al/Cu Layers, *IEEE Journal of selected topics in quantum electronics* **23**, 81 (2017).

[59] Vikas and R. K. Verma, Sensitivity enhancement of a lossy mode resonance based tapered fiber optic sensor with an optimum taper profile, *J. Phys. D: Appl. Phys.* **51**, 415302 (2018).

Figures:

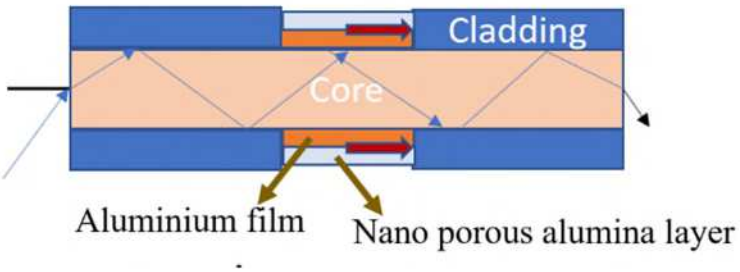

Figure 1: Schematic of the proposed fiber optic probe

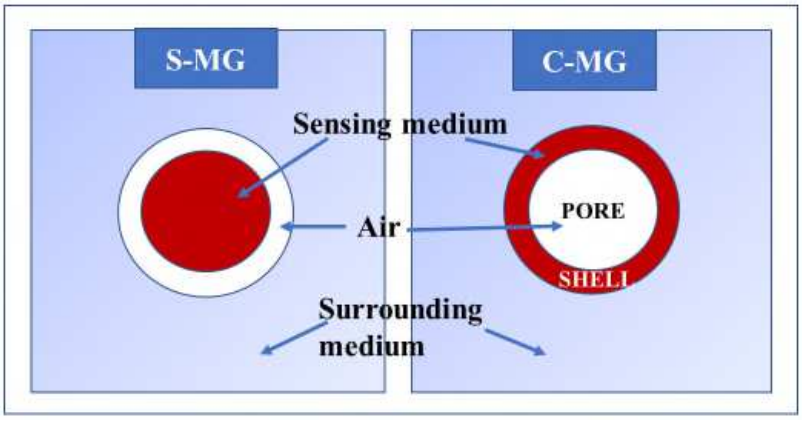

Figure 2: Demonstration of Spherical and Cavity Maxwell Garnet structures

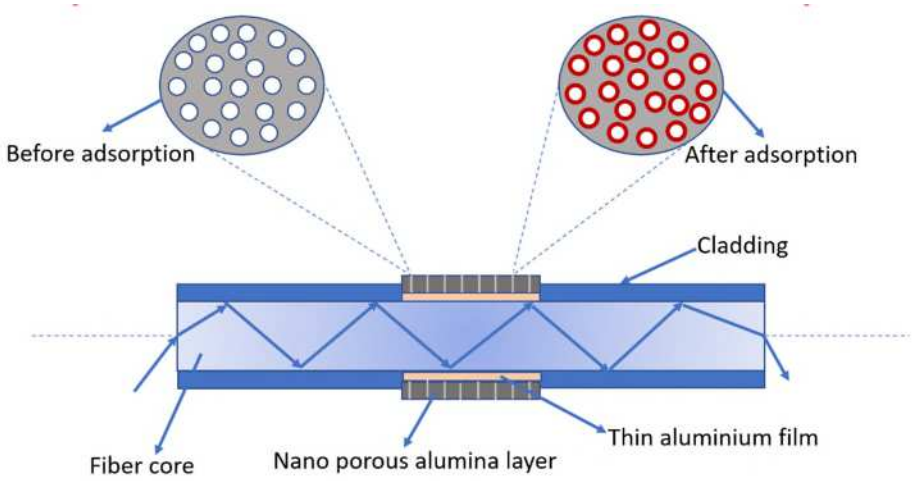

Figure 3: Magnified illustration of the nano-porous alumina surface before and after the formation of a thin layer on the pore walls from horizontal surface

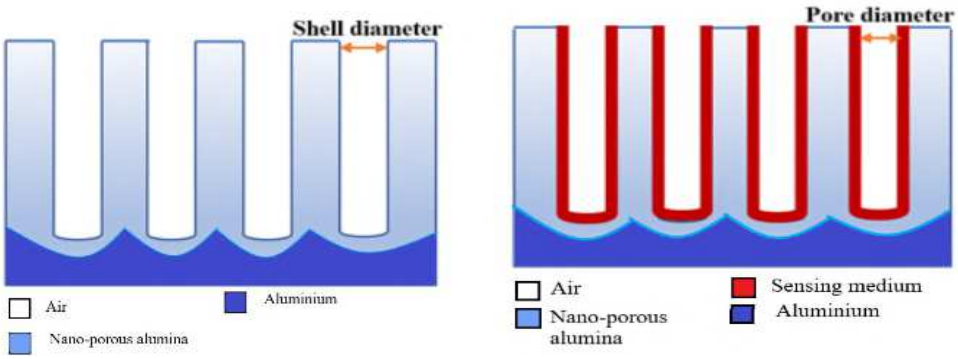

Figure 4: Vertical view of cylindrical nano-porous alumina structure (a) filled with air (b) filled with sensing medium

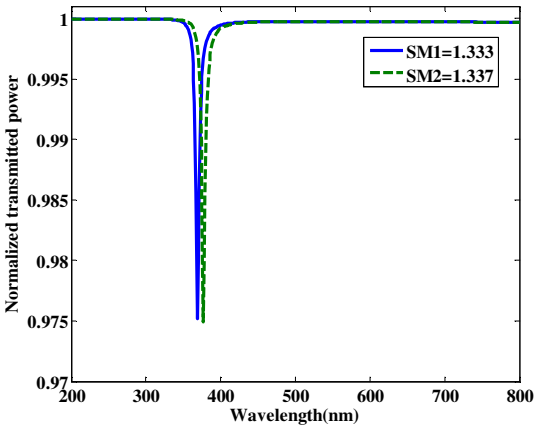

Figure 5: Transmitted power variation for conventional structure with Aluminum film

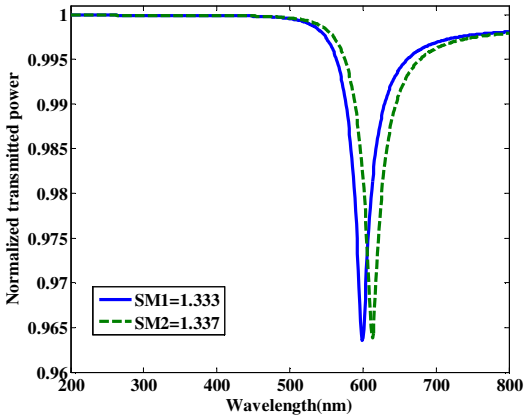

Figure 6: Transmitted power variation for conventional structure with Gold film

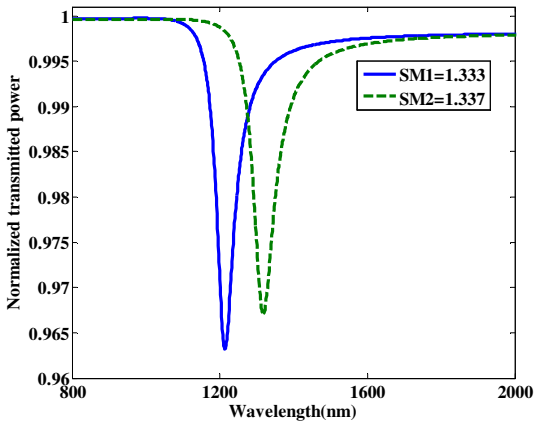

Figure 7: Transmitted power variation for Al film +porous Alumina (Proposed structure)

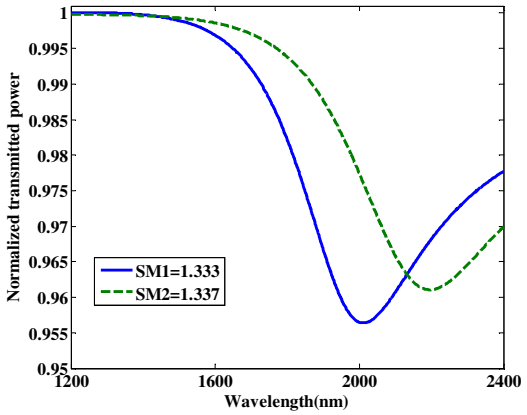

Figure 8: Transmitted power variation for Au film + porous Alumina (Proposed structure)

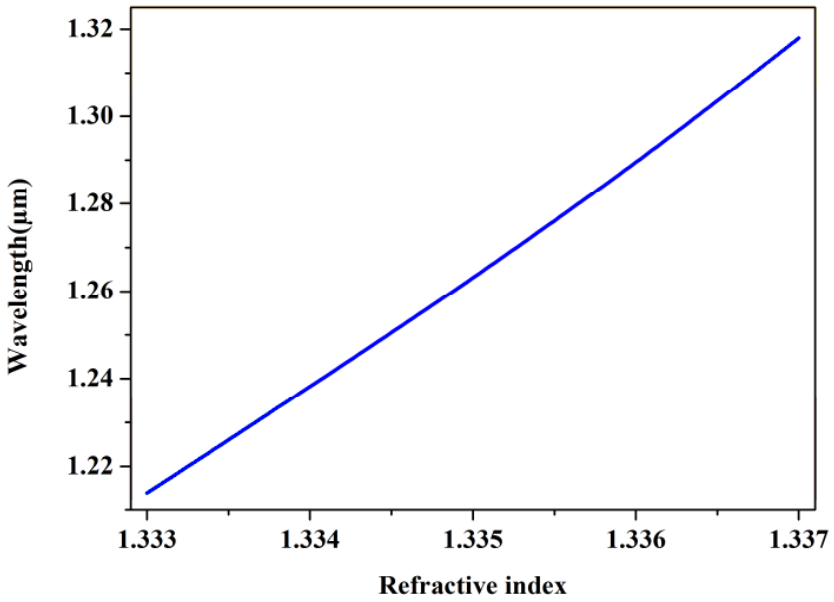

Figure 9: Sensing medium refractive index verses wavelength for Al film + porous alumina

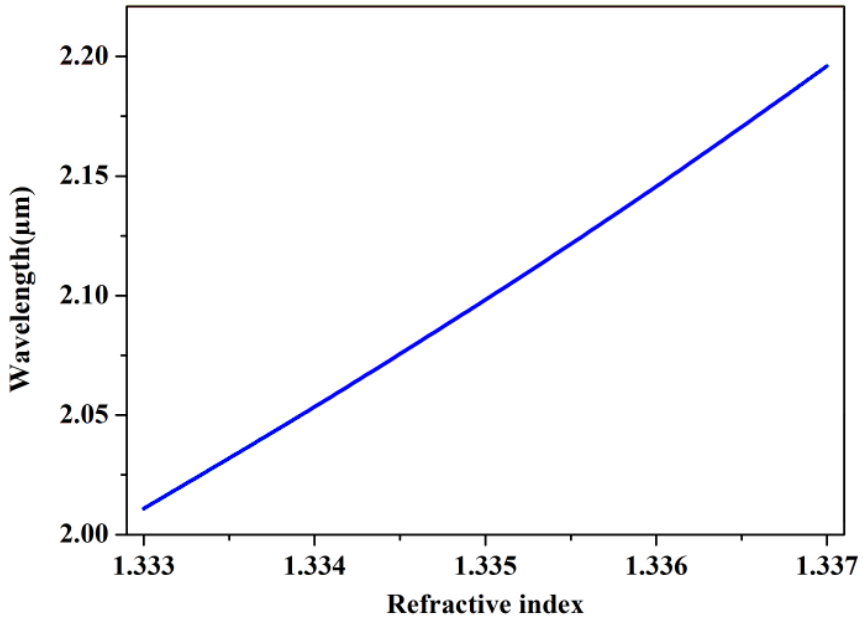

Figure 10: Sensing medium refractive index verses wavelength for Au film + Nano-porous alumina

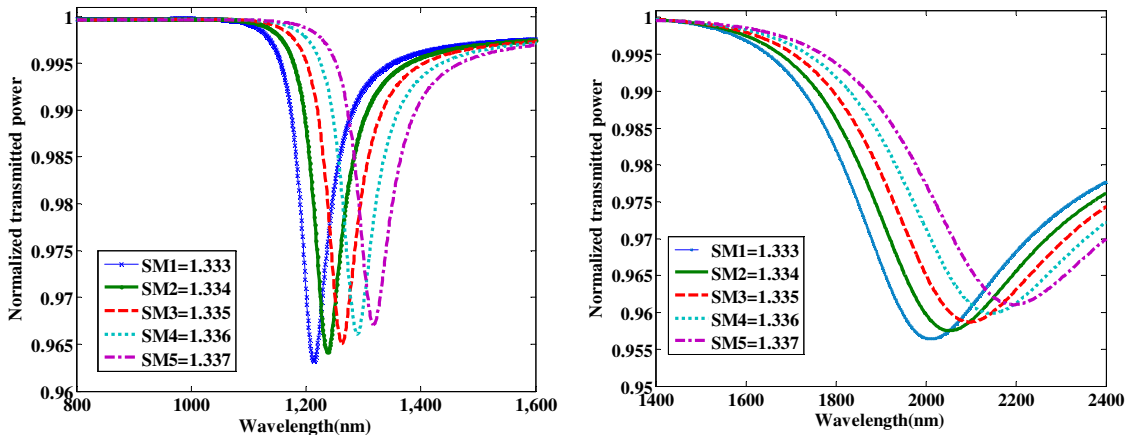

Figure 11: Transmitted power spectrum for different sensing media (a) Al film + porous alumina (b) Au film + porous alumina

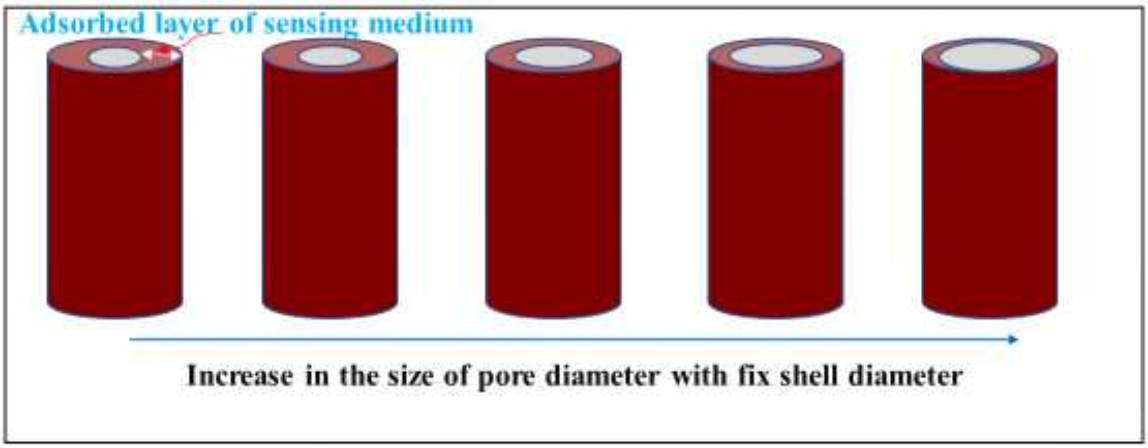

Figure 12: Structural change with variation in pore radius and thickness of sensing medium

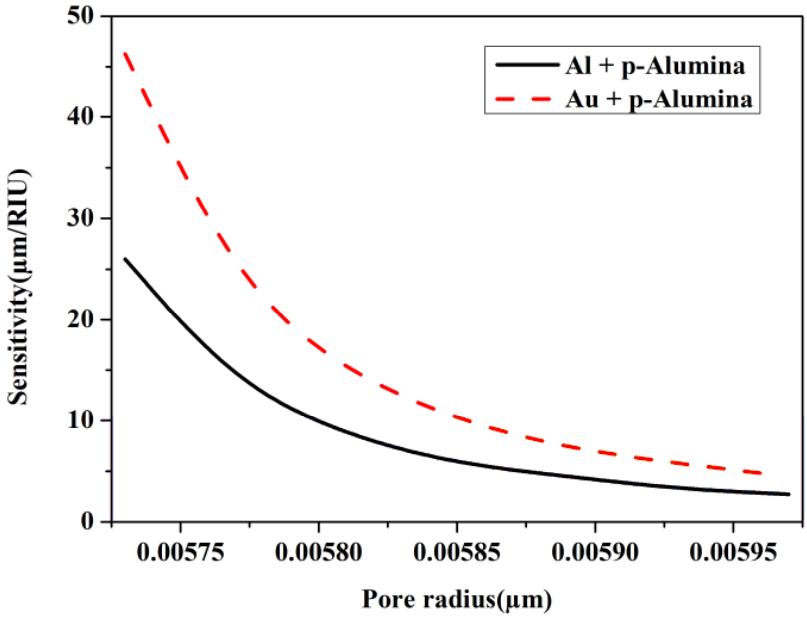

Figure 13: Comparison of Sensitivity for Al film+ porous alumina and Au film+ porous Aluminum structures with Pore radius

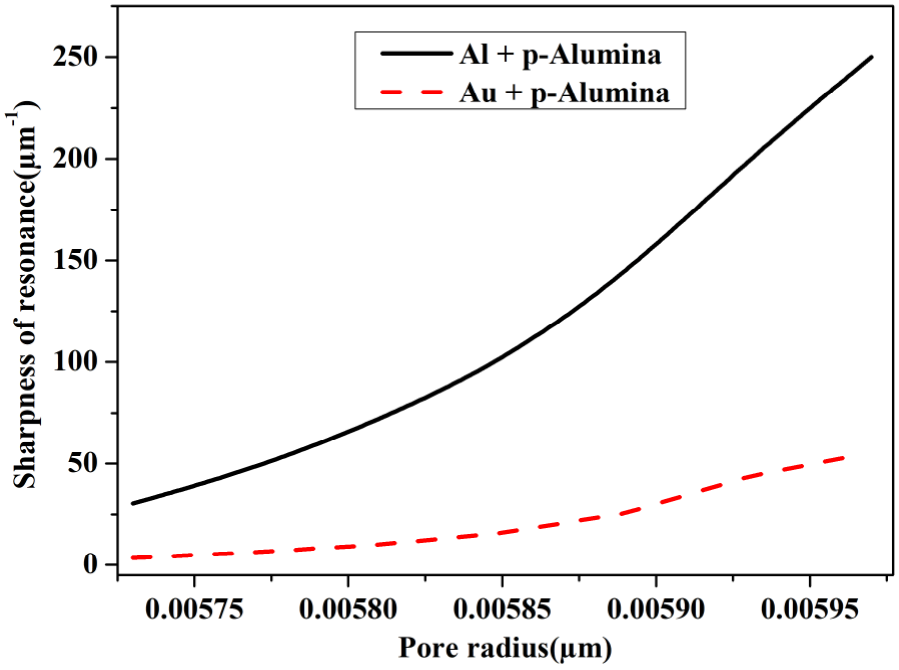

Figure 14: Comparison of Sharpness for Al film+ porous alumina and Au film+ porous Aluminum structures with Pore radius

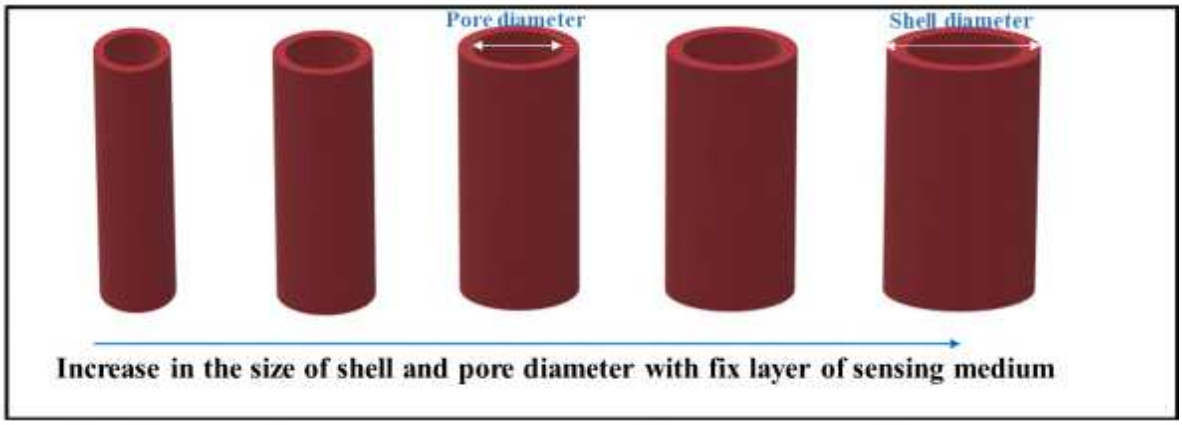

Figure 15: Structural change with variation in pore radius and shell radius with constant thickness of sensing layer

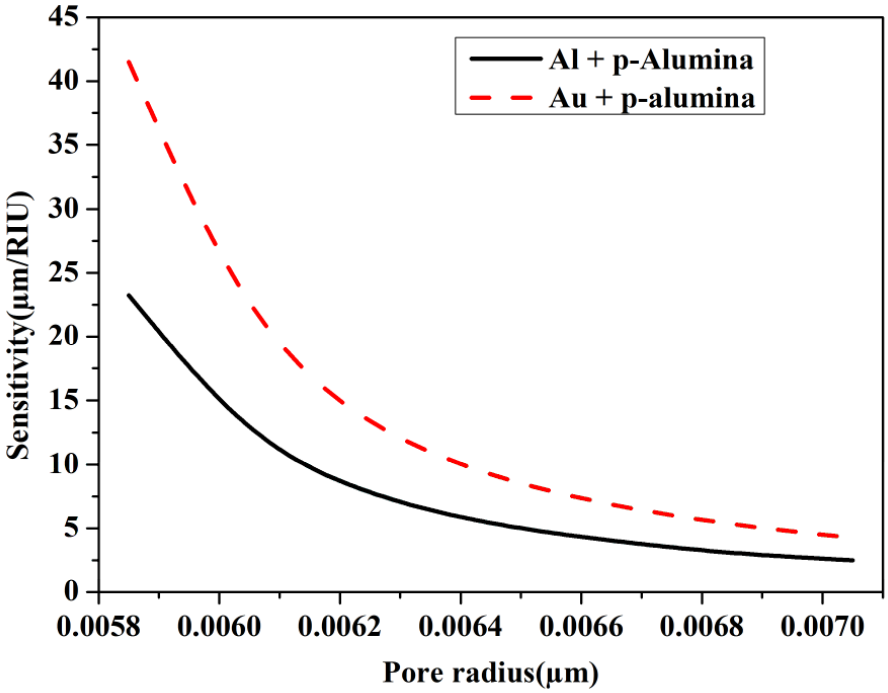

Figure 16: Sensitivity variation with pore radius corresponding to fix sensing layer thickness

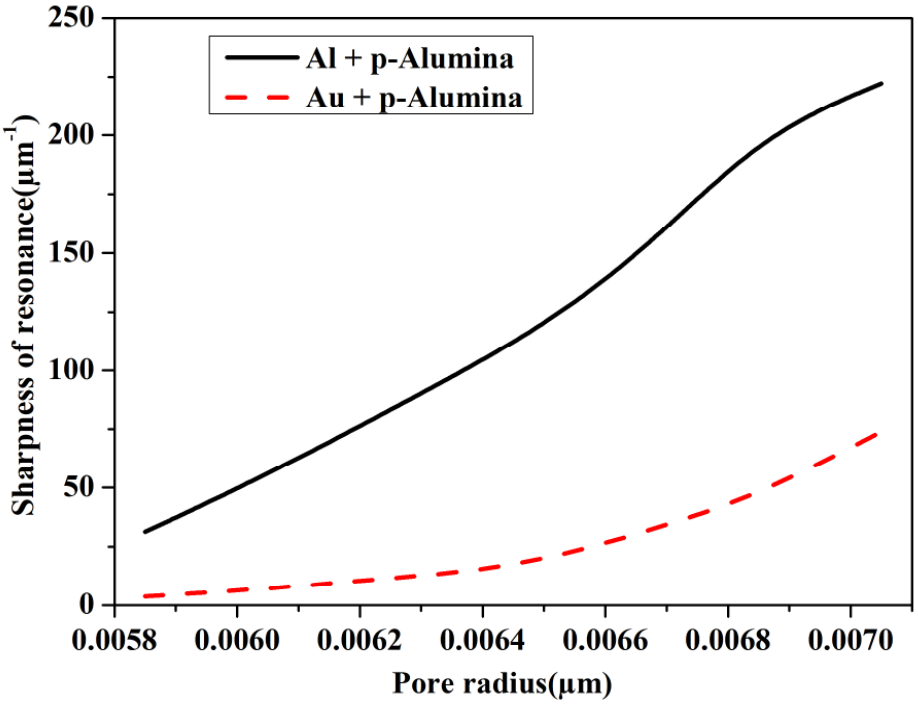

Figure 17: Sharpness of resonance variation with pore radius corresponding to fix sensing layer thickness

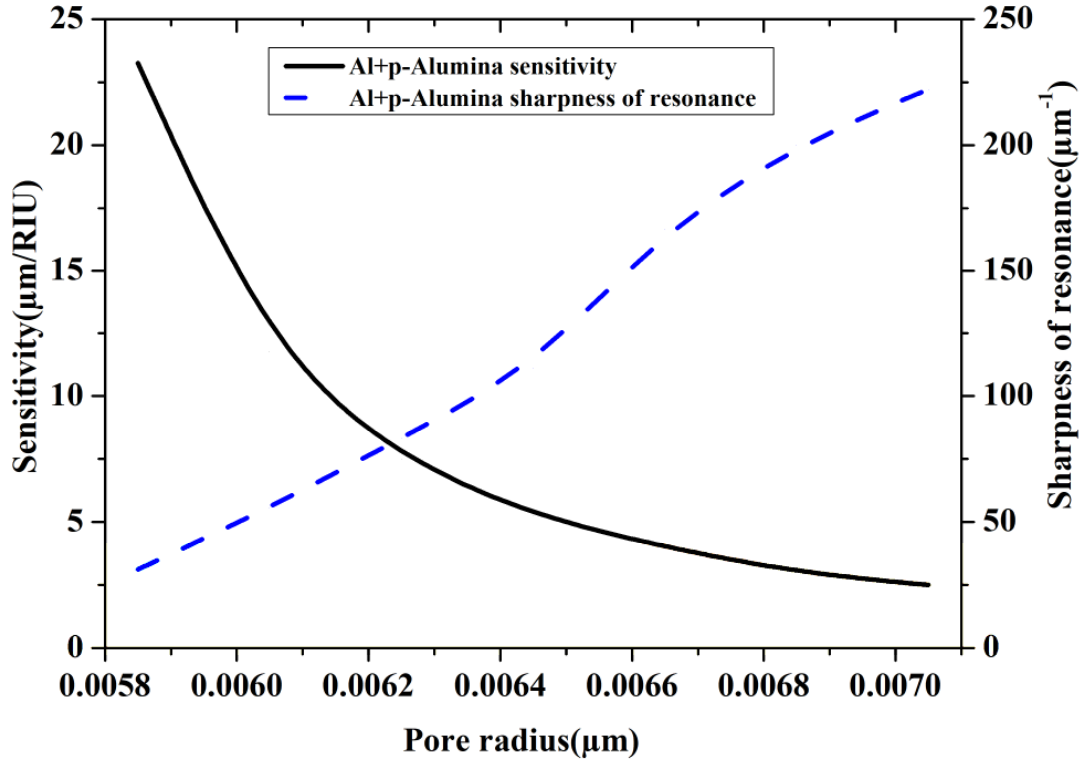

Figure 18: Optimum value of pore radius for reasonably good sensitivity and sharpness of resonance for Al+ porous Alumina

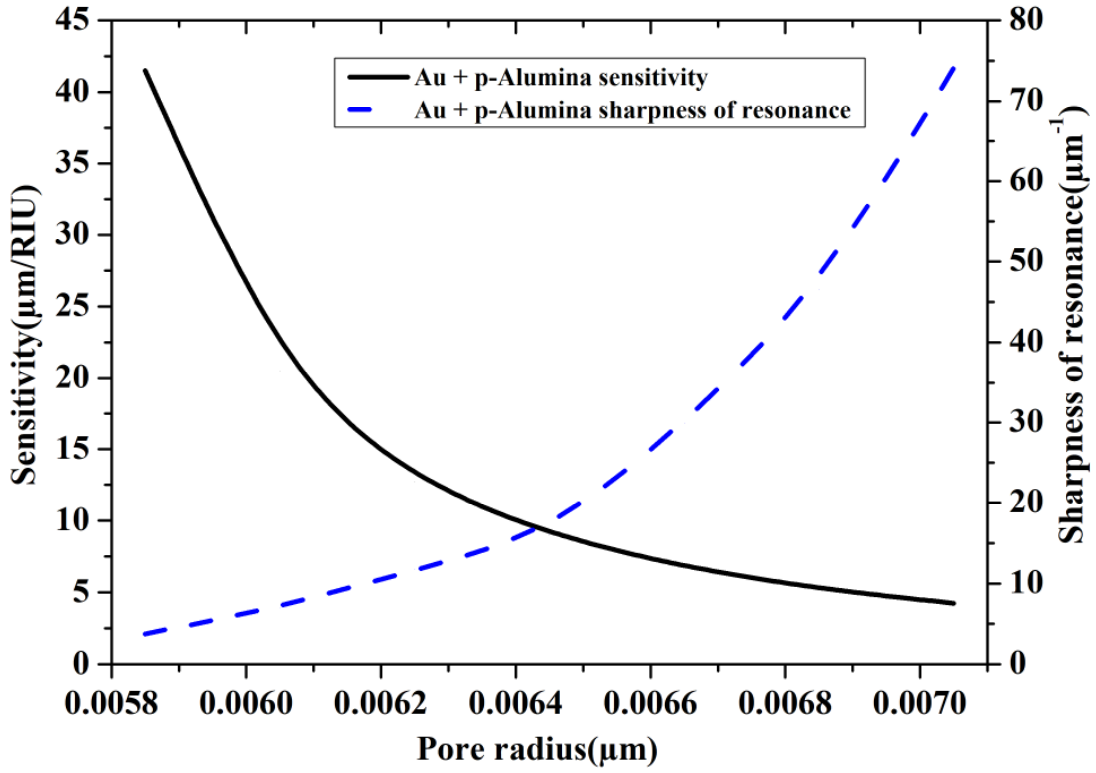

Figure 19: Optimum value of pore radius for reasonably good sensitivity and sharpness of resonance for Au+ porous Alumina

TABLES:

Table 1: Sensitivity values with changing pore radius for fixed shell radius of 0.0075 μm.

Pore radius (μm)	Al sensitivity (μm/RIU)	Au sensitivity (μm/RIU)
0.00573	26	46.25
0.00577	13.5	23.5
0.00581	8.5	14.75
0.00585	5.7	10
0.00589	4.5	7.25
0.00593	3.25	5.75
0.00597	2.75	4.5

Table 2: Sharpness of resonance with pore radius for a fixed shell radius = 0.0075 μm

Pore radius (μm)	Al sharpness of resonance (μm^{-1})	Au sharpness of resonance (μm^{-1})
0.00573	30.3030	3.4364
0.00577	47.619	6.211
0.00581	71.4285	10.1010
0.00585	100	15.87
0.00589	142.8571	25.64
0.00593	200	43.47
0.00597	250	55.55

Table 3: Sensitivity values with pore and shell radius for fix value of the thickness of sensing medium=0.0018 μm

Pore radius (μm)	Shell radius (μm)	Al sensitivity(μm/RIU)	Au sensitivity(μm/RIU)
0.00585	0.00765	23.25	41.5
0.00605	0.00785	11.75	20.5
0.00625	0.00805	7.5	12.75
0.00645	0.00825	5.25	9
0.00665	0.00845	4	6.75
0.00685	0.00865	3	5.25
0.00705	0.00885	2.5	4.25

Table 4: Sharpness of resonance with pore and shell radius for fixed value of thickness of sensing medium=0.0018 μm

Pore radius (μm)	Shell radius (μm)	Al sharpness of resonance (μm^{-1})	Au sharpness of resonance (μm^{-1})
0.00585	0.00765	31.25	3.77
0.00605	0.00785	55.55	7.04
0.00625	0.00805	83.33	11.69
0.00645	0.00825	111.11	16.12
0.00665	0.00845	166.66	29.85
0.00685	0.00865	200	46.511
0.00705	0.00885	222.22	74.07